Low-Energy Spin Excitations in Detwinned FeSe

Ruixian Liu(刘瑞鲜)[1*], Mitsutaka Nakamura[2], Kazuya Kamazawa[3], and Xingye Lu(鲁兴业)[1*]

[1]*Center for Advanced Quantum Studies, School of Physics and Astronomy, Beijing Normal University, Beijing 100875, China*
[2]*J-PARC Center, Japan Atomic Energy Agency (JAEA), Tokai, Ibaraki 319-1195, Japan*
[3]*Research Center for Neutron Science and Technology, Comprehensive Research Organization for Science and Society, Tokai, Ibaraki 319-1106, Japan*

(Received 6 February 2024; accepted manuscript online 8 May 2024)

Antiferromagnetic spin fluctuation is regarded as the leading driving force for electron pairing in high-T_c superconductors. In iron-based superconductors, spin excitations at low energy range, especially the spin-resonance mode at $E_R \sim 5k_BT_c$, are important for understanding the superconductivity. Here, we use inelastic neutron scattering (INS) to investigate the symmetry and in-plane wave-vector dependence of low-energy spin excitations in uniaxial-strain detwinned FeSe. The low-energy spin excitations ($E < 10$ meV) appear mainly at $\boldsymbol{Q} = (\pm 1, 0)$ in the superconducting state ($T \lesssim 9$ K) and the nematic state ($T \lesssim 90$ K), confirming the constant C_2 rotational symmetry and ruling out the C_4 mode at $E \approx 3$ meV reported in a prior INS study. Moreover, our results reveal an isotropic spin resonance in the superconducting state, which is consistent with the $s^{\pm}$ wave pairing symmetry. At slightly higher energy, low-energy spin excitations become highly anisotropic. The full width at half maximum of spin excitations is elongated along the transverse direction. The Q-space isotropic spin resonance and highly anisotropic low-energy spin excitations could arise from d_{yz} intra-orbital selective Fermi surface nesting between the hole pocket around Γ point and the electron pockets centered at M_X point.

DOI: 10.1088/0256-307X/41/6/067401

In iron-based superconductors (FeSCs), superconductivity usually arises from the suppression of the structural transition (T_s) and the antiferromagnetic (AF) order by chemical doping. As the AF order is gradually suppressed, superconductivity emerges and reaches its optimal T_c at the border of the AF regime. Though the AF order vanishes at the optimal doping, intense AF spin fluctuations remain and pervade the whole superconducting regime.[1,2] Due to the intimate correlation between low-energy spin fluctuations and superconductivity, spin excitation has been deemed the leading candidate of the pairing glue for the high-T_c superconductivity in FeSCs.

As a direct response of the low-energy spin excitations $S(\boldsymbol{Q}, E, T)$ to the establishment of superconducting energy gap ($\Delta(T)$), neutron spin resonance mode, defined as $\Delta S(E, T) = S(E, T < T_c) - S(E, T \gtrsim T_c)$ at the AF wave vector, has been proven to be a ubiquitous feature of unconventional superconducting (SC) state, and is one of the most pronounced evidence supporting the picture of spin-fluctuation-driven cooper pairing. The low-energy spin excitations, including spin resonance, are usually interpreted as particle-hole quasiparticle excitations between the hole pockets around the Γ point and the electron pockets around the M point in reciprocal space connected by a finite wave vector $\boldsymbol{k} = (1, 0)$, and favor the sign changing $s^{\pm}$-wave pairing symmetry in FeSCs.[3–6] Moreover, prior studies have shown that both the dispersive high-energy spin excitations associated with localized electronic state and low-energy spin excitations couple with itinerant electrons play essential roles in superconducting pairing.[7–11]

FeSe, with two-dimensional (2D) FeSe layers weakly coupled along the c axis, hosts exotic electronic properties and highly tunable superconductivity.[12–14] The superconducting transition temperature $T_c \approx 9$ K in bulk FeSe can be enhanced to 36.7 K under 8.9 GPa hydrostatic pressure,[15] $\sim$30–46 K when being intercalated by alkali metal or alkaline earth metal ions,[16–18] and even higher than 65 K in monolayer FeSe film grown on $SrTiO_3$.[19–22] Angle resolved photoemission spectroscopy experiments have demonstrated that the extremely shallow Fermi surface with only one ellipse hole pocket is dominated by d_{xz} and d_{yz} characters at the Γ point and a peanut-shaped electron pocket dominated by d_{yz} and d_{xy} characters around the M_X point in the unfolded 1-Fe Brillouin zone in the nematic phase ($T < T_s$) [Fig. 1].[14,23]

Distinct from iron pnictides, FeSe undergoes a tetragonal-to-orthorhombic structural transition at $T_s \approx 90$ K without the formation of static AF order, leaving a unique magnetically disordered electronic nematic state ($T_c < T < T_s$). However, inelastic neutron scattering (INS) and resonant inelastic x-ray scattering (RIXS) experiments have revealed intense spin excitations in FeSe.[24–28] Moreover, the highly anisotropic SC gap and sign-changing $s^{\pm}$ pairing state below T_c also indicate the correlation between superconductivity and AF spin excitations.[5,29,30] Therefore, FeSe provides an ideal platform to understand the intertwining between spin excitations, superconductivity, and electronic nematicity.

However, the orthorhombic lattice distortion below T_s leads to the formation of twin domains, hindering research

*Corresponding authors. Email: liurx@mail.bnu.edu.cn; luxy@bnu.edu.cn
© 2024 Chinese Physical Society and IOP Publishing Ltd

of intrinsic spin excitations and electronic anisotropy in FeSCs.[8,31] To explore the intrinsic electronic properties (spin excitations, etc.), it is necessary to apply a uniaxial pressure/strain along the orthorhombic [100] direction to detwin single crystals. Previously, we used INS and RIXS to explore the intrinsic spin excitations in detwinned FeSe.[25–27] The INS experiment on FeSe detwinned by pressured $BaFe_2As_2$ substrates revealed a puzzling C_4 symmetric low-energy spin excitations at $E = 4 \pm 1$ meV that might correspond to a localized wave vector and energy but has not been well understood.[25] On the other hand, in-plane momentum-space distributions of low-energy spin excitations are connected to the Fermi surface nesting in itinerant picture. The anisotropic low-energy spin excitations (transversely elongated) in $BaFe_{2-x}Ni_xAs_2$ have been well studied, which is in general agreement with random phase approximation (RPA) calculation based on the Fermi surface nesting picture.[32] In FeSe, a similar study will sort out the symmetry and the momentum dependence of the low-energy spin excitations, which, however, is still lacking.

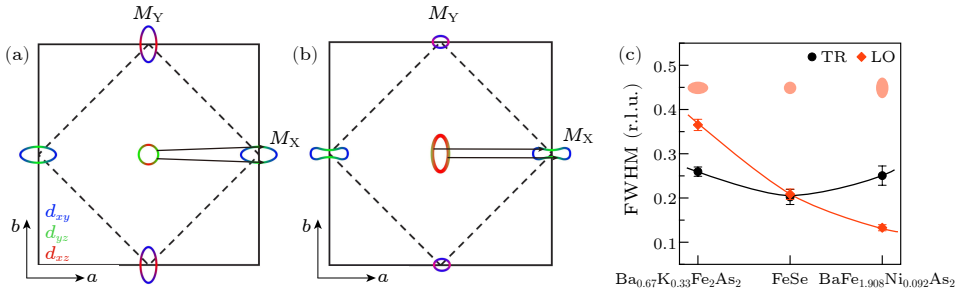

Fig. 1. Schematic of the band structure at $T > T_s$ (a) and at $T < T_s$ (b) in the unfolded 1-Fe Brillouin zone without band hybridizations and spin-orbit coupling.[23] (c) The full width at half maximum (FWHM) of the spin resonance along transverse and longitudinal directions for $Ba_{0.67}K_{0.33}Fe_2As_2$ ($T = 9$ K, $T_c = 38.5$ K), FeSe ($T = 6$ K, $T_c = 9$ K), and $BaFe_{1.908}Ni_{0.092}As_2$ ($T = 3$ K, $T_c = 19$ K).

In this work, we use the same detwinning strategy as in Ref. [27] and have carried out time-of-flight INS experiments to investigate the intrinsic symmetry and in-plane wave-vector dependence of low-energy ($E < 20$ meV) spin excitations in the SC and the normal state.[33,34] Our results revealed the C_2 symmetric spin resonance with $E_R \approx 4$ meV at $\boldsymbol{Q}_{AF} = (\pm 1, 0)$ in the SC state ($T = 6$ K), which is consistent with the previous INS experiment.[25] The intrinsic low-energy spin excitations with $E = 3.5 \pm 0.5$ meV and 4.5 ± 0.5 meV are obviously C_2 symmetric in the normal state at $T = 11$ K, ruling out the existence of the C_4-symmetric spin excitations at $E \approx 3$–5 meV reported in the previous INS experiment.[25] Moreover, the spin resonance induced in the SC state is isotropic in $[H, K]$ plane, in line with the d_{yz} orbital-selective $s^{\pm}$ wave superconducting pairing.[29] In the SC and normal states, low-energy spin excitations at energies higher than spin resonance become highly anisotropic and form transversely elongated ellipses at $\boldsymbol{Q}_1 = (1, 0)$. Our results clarify the symmetry of the low-energy spin excitations in FeSe, the Q-space isotropic spin resonance and anisotropic low-energy spin excitations are consistent with the Fermi surface topology and the d_{yz} orbital selective Fermi surface nesting between the hole and the electron pockets centered at Γ and M_X points of the reciprocal space, respectively.[35]

Experimental Methods. High-quality FeSe single crystals ($T_c \approx 9$ K, $T_s \approx 90$ K) with self-cleaving edges along tetragonal [100] direction were grown using the chemical vapor transport method with KCl-$AlCl_3$ flux as reported elsewhere[36] and characterized by in-plane resistance measurements at a physical property measurement system (PPMS, Quantum Design). For INS experiment, we co-aligned $\sim$1000 pieces of thin FeSe single crystals (total mass ≈ 1.24 g) and glued them onto five aluminum sheets [ten areas, 20×22 mm$^2 \times 5 \times 2$ (sides)] of the uniaxial-strain device using the hydrogen-free CYTOP along tetragonal [100] direction.

To apply uniaxial strain on thousands of pieces of thin FeSe single crystals simultaneously, we use the newly designed uniaxial-strain device consisting of five invar frames and aluminum sheets.[27] Though cooling, the uniaxial strain, produced by the differential thermal expansion coefficients of invar alloy ($\alpha \approx -2 \times 10^{-6}$/K) and aluminum alloy ($\alpha \approx -24 \times 10^{-6}$/K), can be applied on the neck-shaped aluminum sheets along the vertical direction and transferred to FeSe through the CYTOP.[27]

INS measurements were performed on the 4SEASONS time-of-flight spectrometer at the Materials and Life Science Experimental Facility (MLF) in the Japan Proton Accelerator Research Complex (JPARC).[37,38] The incident beam is parallel to the c-axis ($k_i \parallel c$) and the scattering plane is $[H, 0, L]$. We use the multi-E_i mode through the experiment with $E_i = 21$, 36, 80 and 295 meV (Fermi chopper frequency $f = 250$ Hz). Combined with the large detector arrays, we can map out spin excitations over a wide momentum and energy range. Low-energy spin excitations at $T = 6$ K are used to estimate the detwinning ratio ($\eta = [(I_{10} - I_{01})]/[(I_{10} + I_{01})] \approx 58\%$) at $T = 6$ K, where I_{10} and I_{01} represent the integrated intensity of spin excitations at $\boldsymbol{Q} = (1, 0)$ and $(0, 1)$, respectively.

To reduce the neutron scattering background from the device, we use cadmium foils to cover the Invar-alloy frame and empty aluminum sheets in our experiments. In addition, we also used the oscillating radial collimators (ORCs) to reduce scattering signals from sample environment.[39] Throughout this study, orthorhombic notation is used, in which $\boldsymbol{Q}_{AF} = (\pm 1, 0)$ and $(0, \pm 1)$ corresponds to the wave vectors of AF order in twinned FeSCs. More-

over, the wave vector $\boldsymbol{Q}$ in reciprocal space is defined as $\boldsymbol{Q} = H \cdot 2\pi\hat{\boldsymbol{a}}/a_o + K \cdot 2\pi\hat{\boldsymbol{b}}/b_o + L \cdot 2\pi\hat{\boldsymbol{c}}/c_o$, where H, K, L are Miller indices and $a_o \approx 5.33$ Å, $b_o \approx 5.31$ Å, and $c_o \approx 5.49$ Å are lattice parameters in the orthorhombic state.

Results and Discussion. We show the spin resonance of detwinned FeSe in Fig. 2, in which Figs. 2(a) and 2(b) exhibit 2D constant-energy slices of spin excitations with $E = 4 \pm 1$ meV at $T = 6$ K and 11 K, respectively. A $|\boldsymbol{Q}|$-dependent background has been subtracted from the data. In both the SC and the normal state, the intrinsic spin excitations appear only at $\boldsymbol{Q}_1 = (1, 0)$ and show C_2 rotational symmetry. One-dimensional (1D) energy scans at $\boldsymbol{Q}_1 = (1, 0)$ and $\boldsymbol{Q}_2 = (0, 1)$ for $T = 6$ K and 11 K are shown in Figs. 2(c) and 2(d), respectively. The intensity of spin excitations at $\boldsymbol{Q}_1$ is significantly enhanced at $E_R \approx 4$ meV at $T = 6$ K compared with that in the normal state ($T = 11$ K) [Fig. 2(c)], indicating the formation of the spin resonance. By contrast, no obvious enhancement is observed at $\boldsymbol{Q}_2$ in the SC state ($T = 6$ K) [Fig. 2(d)], suggesting the absence of a spin resonance mode at $\boldsymbol{Q}_2$. These results confirm that the spin resonance mode in FeSe appears only at $\boldsymbol{Q}_1$, consistent with previous INS studies.[25,40] Figure 2(e) shows the temperature dependence of 1D constant-energy scans of spin excitations with $E = 4 \pm 1$ meV across $\boldsymbol{Q}_1$. While cooling from 120 K to 11 K reduce the FWHM and enhance the intensity slightly, further cooling across $T_c \approx 9$ K from 11 K to 6 K greatly enhances the intensity of the spin excitations at $\boldsymbol{Q}_1$, corroborating the superconductivity-induced spin resonance as shown in Fig. 2(c).

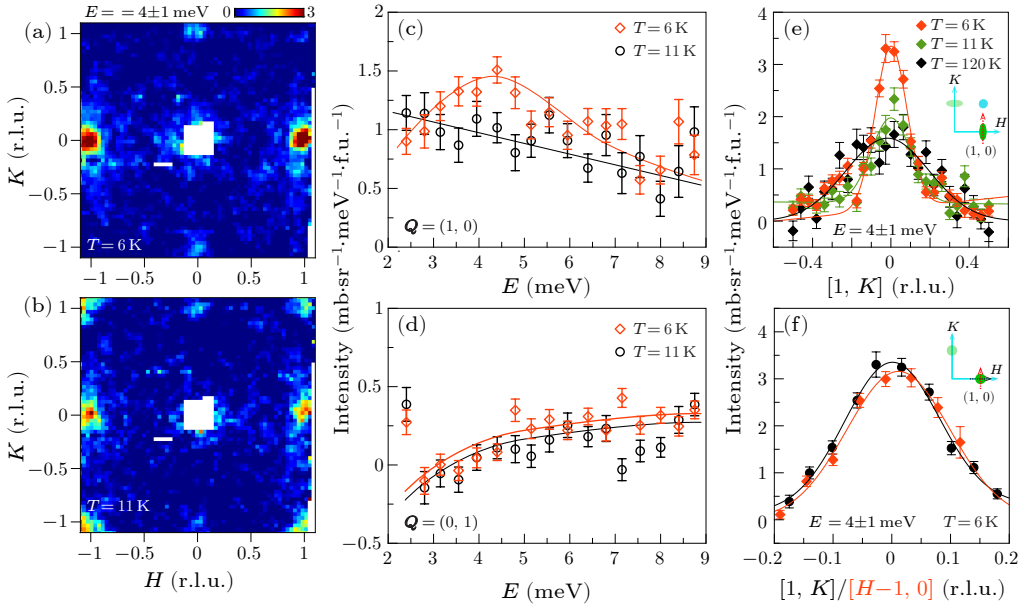

Fig. 2. Two-dimensional constant-energy slices of the spin excitations in detwinned FeSe with $E = 4 \pm 1$ meV at $T = 6$ K (a) and 11 K (b), collected with $E_i = 21$ meV. Low-energy spin excitations at $\boldsymbol{Q}_1 = (1, 0)$ (c) and $\boldsymbol{Q}_2 = (0, 1)$ (d). The red open diamonds and black open circles represent the data measured at $T = 6$ K and 11 K, respectively. The red and black solid lines are guides to the eyes in (c) and (d). (e) Constant energy cuts along transverse direction across $\boldsymbol{Q}_1$ with $E = 4 \pm 1$ meV at $T = 6$ K (red diamonds), 11 K (green diamonds), and 120 K (black diamonds). (f) Constant energy cuts along the transverse direction (black solid circles) and longitudinal direction (red solid diamonds) at $\boldsymbol{Q}_1$ with $E = 4 \pm 1$ meV at $T = 6$ K. The color curves are fittings of the data with Gaussian function in (e) and (f). The $|\boldsymbol{Q}|$-dependent background has been subtracted from the data, and r.l.u. means reduced lattice unit.

Figure 2(f) shows the comparison of the 1D constant-energy cuts measured along the transverse $[1, K]$ direction (black solid circles) and the longitudinal $[H, 0]$ direction (red solid diamonds) at the spin resonance energy $E_R = 4 \pm 1$ meV. The coincidence between these two scans indicates that the spin resonance mode is isotropic in Q space.

Two-dimensional constant-energy slices of the low-energy spin excitations in the normal state ($T = 11$ K) at $E = 3.5 \pm 0.5$ meV, $E = 4.5 \pm 0.5$ meV, $E = 6 \pm 1$ meV, and $E = 8 \pm 1$ meV are shown in Figs. 3(a)–3(d). The scattering intensity at $\boldsymbol{Q}_1$ is much stronger than that at $\boldsymbol{Q}_2$ for all these energies. To further clarify and quantitatively analyze the low-energy spin excitations, we plot the 1D momentum scans along $[1, K]$ and $[H, 1]$ directions across the $\boldsymbol{Q}_1$ and $\boldsymbol{Q}_2$ points at various energies in Figs. 3(e)–3(h). The red and black solid lines are the fitting results of one Gaussian function on a linear background. The spin excitations at $\boldsymbol{Q}_1$ is stronger than that at $\boldsymbol{Q}_2$ in the low-energy range $E = 3$–9 meV.

This again demonstrates that the intrinsic low-energy spin excitations (below T_s) are C_2 symmetric. In the previous INS study of detwinned FeSe (Ref. [25]), a C_4 mode was observed in the energy range $E = 4 \pm 1$ meV at $T = 12$ K. Our results with higher quality demonstrate the absence of this C_4 mode, which might be induced by a background scattering rather than intrinsic spin excitations.

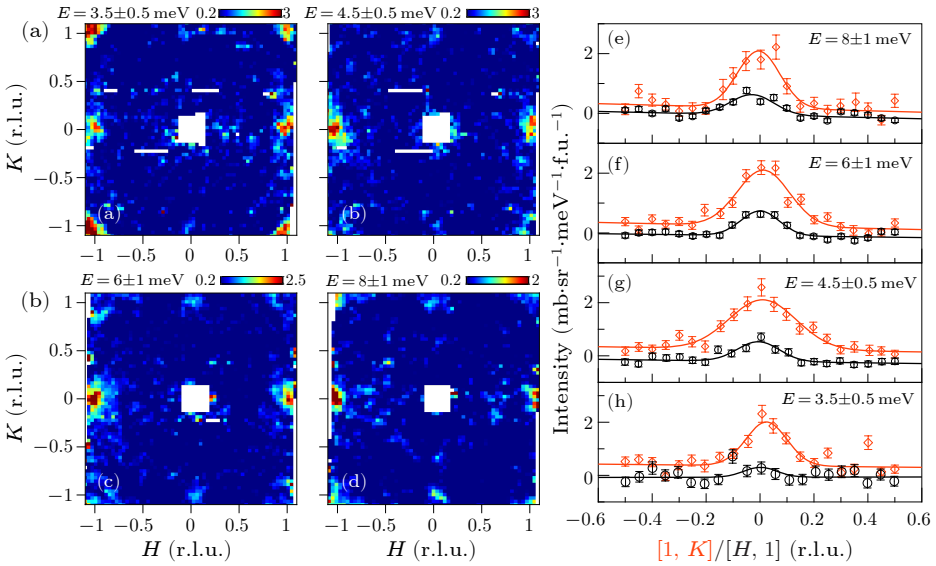

Fig. 3. Low-energy spin excitations of detwinned FeSe at $T = 11$ K: 2D constant-energy slices of the spin excitations in detwinned FeSe with $E = 3.5 \pm 0.5$ meV (a), $E = 4.5 \pm 0.5$ meV (b), $E = 6 \pm 1$ meV (c), and $E = 8 \pm 1$ meV (d), at $T = 11$ K, which are collected with $E_i = 21$ meV. (e)–(h) One-dimensional constant-energy cuts along the [1, K], [H, 1] across $\boldsymbol{Q}_1$ (red open diamonds) and $\boldsymbol{Q}_2$ (black open circles) at $T = 11$ K. The red and black solid curves are fittings of the Gaussian function. The $|\boldsymbol{Q}|$-dependent background has been subtracted from the data (a)–(h).

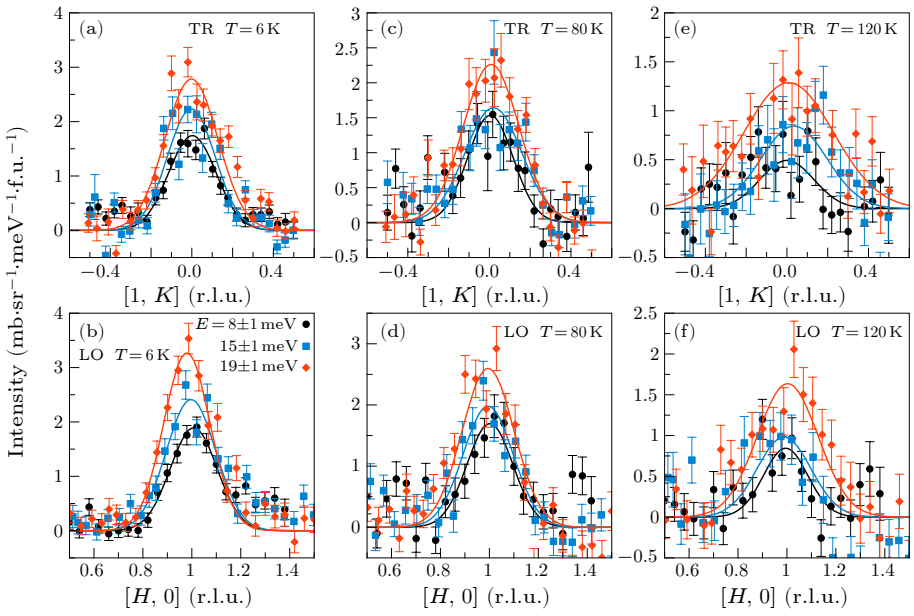

Fig. 4. Energy evolution of spin excitations at $\boldsymbol{Q}_1 = (1, 0)$. Constant energy cuts along the transversal direction [(a), (c), (e)] and longitudinal direction [(b), (d), (f)] with $E = 8 \pm 1$ meV (black solid circles), 15 ± 1 meV (blue solid squares) and 19 ± 1 meV (red solid diamonds) for $T = 6$ K, 80 K, and 120 K. The colored curves are the fitting results of one or two Gaussian functions. The $|\boldsymbol{Q}|$-dependent background has been subtracted from the data.

Momentum Dependence of the Low-Energy Spin Excitations. To show the in-plane wave-vector dependence of low-energy spin excitations in FeSe, we plot 1D constant-energy cuts along the longitudinal (LO) [H, 0] and transverse (TR) [1, K] directions at $\boldsymbol{Q}_1$ with $E = 8 \pm 1$ meV (black solid circles), $E = 15 \pm 1$ meV (blue solid squares) and $E = 19 \pm 1$ meV (red solid diamonds) (Fig. 4). With the increase of the energy, the single commensurate peak centered at $\boldsymbol{Q}_1$ gradually broadens along the TR [Figs. 4(a), 4(c), and 4(e)] and the LO [Figs. 4(b), 4(d), and 4(f)] directions. The low-energy spin excitations broaden more rapidly along the TR direction than the LO direction, leading to elliptically shaped (anisotropic) spin excitations. In addition, we also investigate the temperature dependence of the momentum distribution for the low-energy spin excitations at $T = 6$ K, 90 K, and 120 K in Fig. 5. With increasing temperature, spin excitation peak broadens along TR and LO directions at $\boldsymbol{Q}_1$ for $E = 10.5 \pm 1.5$ meV in Figs. 5(a) and 5(b), $E = 13 \pm 1$ meV in Figs. 5(c) and 5(d), and $E = 17 \pm 1$ meV in Figs. 5(e) and

5(f). The intensity of low-energy spin excitations gradually increases when cooling.

We use the Gaussian function to fit the 1D cuts of the spin excitations shown in Figs. 4 and 5. Figures 6(a) and 6(b) show the energy and temperature dependence of the FWHM extracted from the fitting results. With the energy and temperature increasing, the FWHM shows a linear behavior for both directions (TR and LO). The FWHM along the TR direction is larger than that along the LO direction at $T = 6$ K, which shows minor changes with the increasing energy along both directions, indicating an anisotropy of the spin excitations in this energy range. By contrast, the slope along the TR direction is larger than that along the LO direction at $T = 120$ K, indicating a pronounced anisotropy of the low-energy spin excitations.

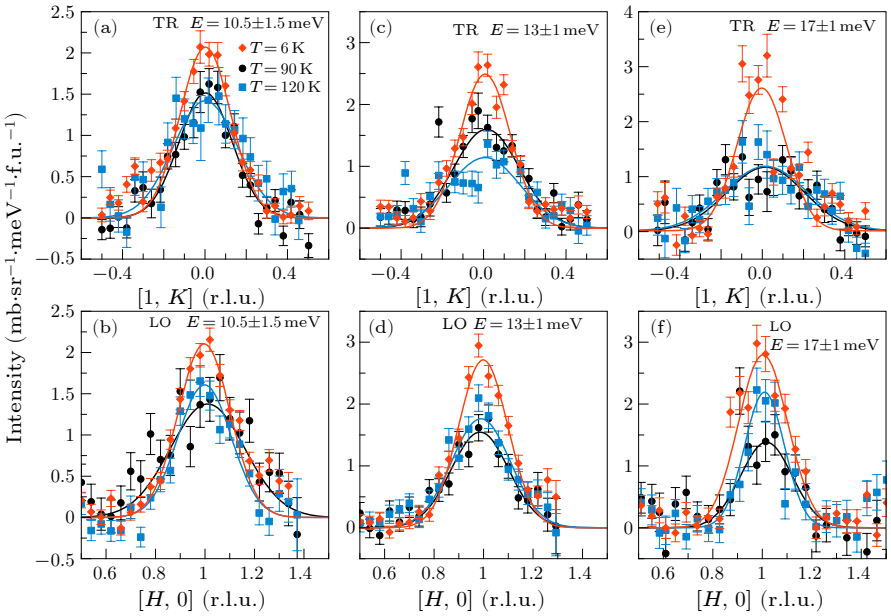

Fig. 5. Temperature evolution of spin excitations at the wave vector $\boldsymbol{Q}_1 = (1, 0)$. Constant energy cuts along the transversal direction [(a), (c), (e)] and longitudinal direction [(b), (d), (f)] at $T = 6$ K (red solid diamonds), 90 K (black solid circles), and 120 K (blue solid squares) with $E = 10.5 \pm 1.5$ meV [(a), (b)], $E = 13 \pm 1$ meV [(c), (d)] and $E = 17 \pm 1$ meV [(e), (f)]. The colored curves are the fitting results of one or two Gaussian functions. The $|\boldsymbol{Q}|$-dependent background has been subtracted from the data.

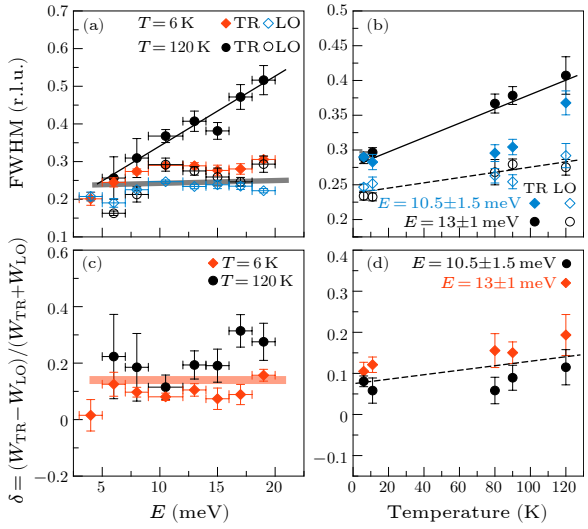

Fig. 6. Energy dependence of FWHM for TR and LO cuts (a) and in-plane spin excitation anisotropy δ (c) at $Q = (1, 0)$ for $T = 6$ K and 120 K. Temperature dependence of FWHM for the TR and LO cuts (b) and in-plane spin excitation anisotropy (d) at $\boldsymbol{Q}_1 = (1, 0)$ with $E = 10.5 \pm 1.5$ meV and $E = 13 \pm 1$ meV ($E_i = 36$ meV).

Note that the LO and the TR cuts of the spin resonance ($E = 4 \pm 1$ meV, $T = 6$ K) almost coincide with each other with similar FWHM (TR: 0.19 ± 0.02 r.l.u.; LO: 0.21 ± 0.012 r.l.u.) and intensity, indicating an isotropic spin resonance in FeSe.

We define the anisotropy of the spin excitation at $\boldsymbol{Q}_1$ as $\delta = (W_{TR} - W_{LO})/(W_{TR} + W_{LO})$, where W_{TR} and W_{LO} are the FWHMs of spin excitations along the TR and the LO directions, respectively. Figure 6(c) shows that the spin excitation anisotropy δ is close to 0 at E_R (isotropic spin resonance) at $T = 6$ K, which becomes obviously larger than 0 for higher energies ($E = 5$–20 meV). When warming from $T = 6$ K to 120 K, the anisotropy δ for $E = 10.5 \pm 1.5$ meV ($E = 13 \pm 1$ meV) increases slightly from 0.08 (0.11) to 0.11 (0.19) [Fig. 6(d)]. For $E \gtrsim 14$ meV, δ becomes even larger at $T = 120$ K.

Different from cuprates governed by Mott physics, FeSCs are multi-orbital Hund's metals and exhibit various itinerant electronic properties. In itinerant picture, AF spin excitations and superconductivity are suggested to be associated with Fermi surface nesting between the hole pockets at the Γ point and the electron pockets at the $M_{X/Y}$ points. The in-plane anisotropy of spin excitations has been discovered in various FeSCs, such as $CaFe_2As_2$,[41] electron-doped $Ba(Fe_{1-x}Ni_x)_2As_2$,[32] $Ba(Fe_{1-x}Co_x)_2As_2$,[11,42–44] and hole-doped $Ba_{0.67}K_{0.33}Fe_2As_2$,[34] with the magnitude

and sign of δ depending on Fermi surface topology and orbital characters, as the low-energy spin excitations arise from intra-orbital scattering between the hole and the electron pockets.

In doped $BaFe_2As_2$ systems, the hole pockets shrink (expand) with electron (hole) doping, and the electron pockets evolve with the opposite trend. The spin resonance elongated along the TR direction in electron-doped $BaFe_2As_2$ [Fig. 1(c)], such as $Ba(Fe_{1-x}Co_x)_2As_2$ and $Ba(Fe_{1-x}Ni_x)_2As_2$, is interpreted as the d_{yz} intra-orbital scattering from Γ to M_X, which favors the fully gapped $s^{\pm}$ pairing state.[11,32,44,45] Such a d_{yz} orbital-selective Fermi surface nesting picture has also been used to explain the spin resonance elongated along the LO direction [Fig. 1(c)] in hole-doped $BaFe_2As_2$ (such as $Ba_{0.67}K_{0.33}Fe_2As_2$). The distinct Fermi surface topology gives rise to the finite offset along the LO direction.[34,42]

In detwinned FeSe, there is only one hole pocket at the Γ point and one electron pocket at the M point in the unfolded 1-Fe Brillouin zone without band hybridizations and spin-orbit coupling in tetragonal phase ($T > T_s = 90\,K$) [Fig. 1(a)]. In the nematic phase ($T < T_s$), the Fermi surface evolves into an elliptical-shaped hole pocket at the Γ point and a peanut-shaped electron pocket at the M point [Fig. 1(b)].[12,23] Based on similar Fermi surface topology, dynamical mean field theory (DMFT) and density functional theory (DFT) calculation of the spin excitations in the tetragonal state suggest that the excitations at $E = 5\,meV$ are highly anisotropic in $[H, K]$ space $W_{TR}/W_{LO} \gtrsim 2$. These results are qualitatively consistent with our anisotropic low-energy spin excitations measured at $T = 120\,K > T_s$. This consistency shows that the spin excitations arise from d_{yz} intra-orbital scattering between the hole pocket at (0, 0) and the electron pocket at (1, 0). In the tetragonal phase, the nesting wave-vector is offset from $\boldsymbol{Q}_1 = (1, 0)$ by a finite ΔQ_y driven by the intra-orbital scattering (with $\Delta E = 5$–$20\,meV$) from d_{yz} orbitals, which induces a commensurate peak elongated slightly along the TR direction.

When cooling across T_s and T_c, the spin excitation anisotropy δ decreases and the spin resonance (at $T < T_c$) in FeSe is isotropic. The nematic phase modifies the Fermi surface, leading to the elongated hole pocket at Γ, and the peanut-shaped electron pocket at M_X. In the previous neutron and Bogoliubov quasiparticle interference imaging experiments,[25,29,40] superconductivity and spin excitations in FeSe are proven to arise from the d_{yz} orbital of the Fe atoms, consistent with our experimental measurements. In this scenario, RPA calculation can be employed to describe the highly anisotropic superconducting energy gap of FeSe,[29] and the calculated spin resonance is slightly longitudinally elongated.[25] This is close to the isotropic spin resonance observed in our experiment, which corroborates the origin of the spin resonance, i.e., the d_{yz} orbital-selective spin fluctuations driven by the Fermi surface nesting between Γ and M_X. We argue that the difference (slightly elongated in calculation but isotropic in INS) could still provide new insights into understanding the formation of the spin resonance.

Qualitatively, combined with the shape of the Fermi surface (taken from Ref. [23]), the nesting wave-vector between d_{yz} orbitals is offset by a finite ΔQ_y and at the same time offset by a finite ΔQ_x. When ΔQ_y is equivalent to ΔQ_x, the spin excitations will be isotropic. Moreover, the spin excitations at $T > T_s$ become much broader than that at $T < T_s$ along the TR direction, along with the change of electronic structure above and below T_s. Therefore, both the anisotropic low-energy spin excitations and isotropic spin resonance in FeSe arise from the d_{yz} intra-orbital scattering via a wave vector $\boldsymbol{Q}$ between the hole pocket at Γ and the electron pocket at M point of the reciprocal space.[8]

In summary, we have investigated the symmetry and the in-plane wave-vector dependence of the intrinsic low-energy spin excitations by performing the INS experiments on detwinned FeSe. The intrinsic low-energy spin excitations at $E = 3.5 \pm 0.5\,meV$, $E = 4.5 \pm 0.5\,meV$, $E = 6 \pm 1\,meV$, and $E = 8 \pm 1\,meV$, including spin resonance ($E \approx 4\,meV$) with C_2 rotational symmetry appears only at $\boldsymbol{Q}_1 = (\pm 1, 0)$. Our results rule out the existence of the C_4 spin excitation mode in the normal state. The Q-space isotropic spin resonance in the SC state and highly anisotropic low-energy spin excitations are associated with the d_{yz} intra-orbital scattering.

Acknowledgements. The work at Beijing Normal University was supported by the Fundamental Research Funds for the Central Universities, the National Key Projects for Research and Development of China (No. 2021YFA1400400), and the National Natural Science Foundation of China (Grant Nos. 12174029 and 11922402). We acknowledge the neutron beamtimes from J-PARC (Proposal No. 2019A0002).

References

[1] Chen X H, Dai P C, Feng D L, Xiang T, and Zhang F C 2014 *Nat. Sci. Rev.* **1** 371
[2] Kordyuk A A 2012 *Low Temp. Phys.* **38** 888
[3] Inosov D S, Park J T, Charnukha A, Li Y, Boris A V, Keimer B, and Hinkov V 2011 *Phys. Rev. B* **83** 214520
[4] Yu G, Li Y, Motoyama E M, and Greven M 2009 *Nat. Phys.* **5** 873
[5] Hirschfeld P J, Korshunov M M, and Mazin I I 2011 *Rep. Prog. Phys.* **74** 124508
[6] Hong W, Song L, Liu B, Li Z, Zeng Z, Li Y, Wu D, Sui Q, Xie T, Danilkin S, Ghosh H, Ghosh A, Hu J, Zhao L, Zhou X, Qiu X, Li S, and Luo H 2020 *Phys. Rev. Lett.* **125** 117002
[7] Scalapino D J 2012 *Rev. Mod. Phys.* **84** 1383
[8] Dai P 2015 *Rev. Mod. Phys.* **87** 855
[9] Wang M, Zhang C, Lu X, Tan G, Luo H, Song Y, Wang M, Zhang X, Goremychkin E A, Perring T G, Maier T A, Yin Z, Haule K, Kotliar G, and Dai P 2013 *Nat. Commun.* **4** 2874
[10] Yin Z P, Haule K and Kotliar G 2014 *Nat. Phys.* **10** 845
[11] Li H F, Broholm C, Vaknin D, Fernandes R M, Abernathy D L, Stone M B, Pratt D K, Tian W, Qiu Y, Ni N, Diallo S O, Zarestky J L, Bud'ko S L, Canfield P C, and McQueeney R J 2010 *Phys. Rev. B* **82** 140503
[12] Coldea A I and Watson M D 2018 *Annu. Rev. Condens. Matter Phys.* **9** 125
[13] Böhmer A E and Kreisel A 2018 *J. Phys.: Condens. Matter* **30** 023001
[14] Shibauchi T, Hanaguri T, and Matsuda Y 2020 *J. Phys. Soc. Jpn.* **89** 102002

[15] Medvedev S, McQueen T M, Troyan I A, Palasyuk T, Eremets M I, Cava R J, Naghavi S, Casper F, Ksenofontov V, Wortmann G, and Felser C 2009 *Nat. Mater.* **8** 630

[16] Ying T P, Chen X L, Wang G, Jin S F, Zhou T T, Lai X F, Zhang H, and Wang W Y 2012 *Sci. Rep.* **2** 426

[17] Krzton-Maziopa A, Shermadini Z, Pomjakushina E, Pomjakushin V, Bendele M, Amato A, Khasanov R, Luetkens H, and Conder K 2011 *J. Phys.: Condens. Matter* **23** 052203

[18] Guo J, Jin S, Wang G, Wang S, Zhu K, Zhou T, He M, and Chen X 2010 *Phys. Rev. B* **82** 180520

[19] Ge J F, Liu Z L, Liu C H, Gao C L, Qian D, Xue Q K, Liu Y, and Jia J F 2015 *Nat. Mater.* **14** 285

[20] Wang Q Y, Li Z, Zhang W H, Zhang Z C, Zhang J S, Li W, Ding H, Ou Y B, Deng P, Chang K, Wen J, Song C L, He K, Jia J F, Ji S H, Wang Y Y, Wang L L, Chen X, Ma X C, and Xue Q K 2012 *Chin. Phys. Lett.* **29** 037402

[21] He S L, He J F, Zhang W H, Zhao L, Liu D F, Liu X, Mou D X, Ou Y B, Wang Q Y, Li Z, Wang L L, Peng Y Y, Liu Y, Chen C Y, Yu L, Liu G D, Dong X L, Zhang J, Chen C T, Xu Z Y, Chen X, Ma X C, Xue Q K, and Zhou X J 2013 *Nat. Mater.* **12** 605

[22] Tan S Y, Zhang Y, Xia M, Ye Z R, Chen F, Xie X, Peng R, Xu D F, Fan Q, Xu H C, Jiang J, Zhang T, Lai X C, Xiang T, Hu J P, Xie B P, and Feng D L 2013 *Nat. Mater.* **12** 634

[23] Yi M, Pfau H, Zhang Y, He Y, Wu H, Chen T, Ye Z R, Hashimoto M, Yu R, Si Q, Lee D H, Dai P C, Shen Z X, Lu D H, and Birgeneau R J 2019 *Phys. Rev. X* **9** 041049

[24] Wang Q, Shen Y, Pan B, Hao Y, Ma M, Zhou F, Steffens P, Schmalzl K, Forrest T R, Abdel-Hafiez M, Chen X, Chareev D A, Vasiliev A N, Bourges P, Sidis Y, Cao H, and Zhao J 2016 *Nat. Mater.* **15** 159

[25] Chen T, Chen Y, Kreisel A, Lu X, Schneidewind A, Qiu Y, Park J T, Perring T G, Stewart J R, Cao H, Zhang R, Li Y, Rong Y, Wei Y, Andersen B M, Hirschfeld P J, Broholm C, and Dai P 2019 *Nat. Mater.* **18** 709

[26] Lu X Y, Zhang W L, Tseng Y, Liu R X, Tao Z, Paris E, Liu P P, Chen T, Strocov V N, Song Y, Yu R, Si Q M, Dai P C, and Schmitt T 2022 *Nat. Phys.* **18** 806

[27] Liu R X, Stone M B, Gao S, Nakamura M, Kamazawa K, Krajewska A, Walker H C, Cheng P, Yu R, Si Q M, Dai P C, and Lu X Y 2024 arXiv:2401.05092 [cond-mat.supr-con]

[28] Wang Q, Shen Y, Pan B, Zhang X, Ikeuchi K, Iida K, Christianson A D, Walker H C, Adroja D T, Abdel-Hafiez M, Chen X, Chareev D A, Vasiliev A N, and Zhao J 2016 *Nat. Commun.* **7** 12182

[29] Sprau P O, Kostin A, Kreisel A, Böhmer A E, Taufour V, Canfield P C, Mukherjee S, Hirschfeld P J, Andersen B M, and Davis J C S 2017 *Science* **357** 75

[30] Hirschfeld P J, Altenfeld D, Eremin I, and Mazin I I 2015 *Phys. Rev. B* **92** 184513

[31] Tanatar M A, Kreyssig A, Nandi S, Ni N, Bud'ko S L, Canfield P C, Goldman A I, and Prozorov R 2009 *Phys. Rev. B* **79** 180508

[32] Luo H, Yamani Z, Chen Y, Lu X, Wang M, Li S, Maier T A, Danilkin S, Adroja D T, and Dai P 2012 *Phys. Rev. B* **86** 024508

[33] Zhang J, Sknepnek R, and Schmalian J 2010 *Phys. Rev. B* **82** 134527

[34] Zhang C L, Wang M, Luo H Q, Wang M Y, Liu M S, Zhao J, Abernathy D L, Maier T A, Marty K, Lumsden M D, Chi S X, Chang S, Rodriguez-Rivera J A, Lynn J W, Xiang T, Hu J P, and Dai P C 2011 *Sci. Rep.* **1** 115

[35] Graser S, Kemper A F, Maier T A, Cheng H P, Hirschfeld P J, and Scalapino D J 2010 *Phys. Rev. B* **81** 214503

[36] Yan J Q, Sales B C, Susner M A, and McGuire M A 2017 *Phys. Rev. Mater.* **1** 023402

[37] Kajimoto R, Nakamura M, Inamura Y, Mizuno F, Nakajima K, Ohira-Kawamura S, Yokoo T, Nakatani T, Maruyama R, Soyama K, Shibata K, Suzuya K, Sato S, Aizawa K, Arai M, Wakimoto S, Ishikado M, Shamoto S i, Fujita M, Hiraka H, Ohoyama K, Yamada K, and Lee C H 2011 *J. Phys. Soc. Jpn.* **80** SB025

[38] Seto H, Itoh S, Yokoo T, Endo H, Nakajima K, Shibata K, Kajimoto R, Ohira-Kawamura S, Nakamura M, Kawakita Y, Nakagawa H, and Yamada T 2017 *Biochimica et Biophysica Acta-General Subjects* **1861** 3651

[39] Nakamura M, Kambara W, Iida K, Kajimoto R, Kamazawa K, Ikeuchi K, Ishikado M, and Aoyama K 2018 *Physica B* **551** 480

[40] Chen T, Chen Y Z, Tam D W, Gao B, Qiu Y M, Schneidewind A, Radelytskyi I, Prokes K, Chi S X, Matsuda M, Broholm C, and Dai P C 2020 *Phys. Rev. B* **101** 140504

[41] Diallo S O, Pratt D K, Fernandes R M, Tian W, Zarestky J L, Lumsden M, Perring T G, Broholm C L, Ni N, Bud'ko S L, Canfield P C, Li H F, Vaknin D, Kreyssig A, Goldman A I, and McQueeney R J 2010 *Phys. Rev. B* **81** 214407

[42] Park J T, Inosov D S, Yaresko A, Graser S, Sun D L, Bourges P, Sidis Y, Li Y, Kim J H, Haug D, Ivanov A, Hradil K, Schneidewind A, Link P, Faulhaber E, Glavatskyy I, Lin C T, Keimer B, and Hinkov V 2010 *Phys. Rev. B* **82** 134503

[43] Lester C, Chu J H, Analytis J G, Perring T G, Fisher I R, and Hayden S M 2010 *Phys. Rev. B* **81** 064505

[44] Tian L, Liu P P, Xu Z, Li Y, Lu Z L, Walker H C, Stuhr U, Tan G T, Lu X Y, and Dai P C 2019 *Phys. Rev. B* **100** 134509

[45] Liu M, Harriger L W, Luo H, Wang M, Ewings R A, Guidi T, Park H, Haule K, Kotliar G, Hayden S M, and Dai P 2012 *Nat. Phys.* **8** 376